Numerical simulation of crust freezing in processed meat: a fully coupled solid-fluid approach

Evaldas Greiciunas, Federico Municchi, Nicodemo Di Pasquale, and *Matteo Icardi

School of Mathematical Sciences, University of Nottingham, NG7 2RD, UK

Abstract

We present a numerical model for the simulation of continuous impingement freezing of processed food products. This model is capable of fully describing the fluid dynamics of the non-isothermal flow field, including turbulence with conjugate heat transfer (CHT). The motion of the solid region is captured by advecting the solid rathe than employing a moving mesh algorithm, resulting in a model that is more computationally efficient. This methodology is implemented as a numerical solver using the well-known open-source library OpenFOAM. Our results confirm that the proposed model can provide detailed insight on the freezing process at a minimum computational cost.

*Corresponding author: Matteo.Icardi@nottingham.ac.uk

Nomenclature

α_{eff}	Effective thermal diffusivity of the fluid [m^2/s]
α_{s}	Thermal diffusivity of the solid [m^2/s]
$\dot{q}_{fs}$	Interface heat flux [W/m^2]
κ	Thermal conductivity [W/(m K)]
$\mathbf{u}$	Fluid velocity field [m/s]
$\mathbf{v}$	Conveyor velocity [m/s]
μ	Fluid viscosity [Pa s]
μ_{eff}	Effective viscosity [Pa s]
ρ_{f}	Fluid density [kg/m^3]
ρ_{s}	Solid density [kg/m^3]
τ_w	Wall shear stress [Pa]
τ_{eff}	Effective shear stress [Pa]
Pe_{s}	Péclet number of the solid
Cp	Specific heat [$W/(m^2$ K)]
Fr	Frozen crust
h_{f}	Fluid enthalpy [J/Kg]
h_{s}	Solid enthalpy [J/Kg]
p_{rgh}	Pressure head [Pa]
T	Temperature [K]
t_{fz}	Dimensionless freezing time
$T_{in,\text{f}}$	Jet temperature at the inlet [K]
T_{sf}	Mean temperature at the fluid-solid interface [K]
U_{in}	Jet inlet velocity [m/s]
x_{fz}	Axial frozen coordinate [m]
y^+	Shear wall distance
y_{fz}	Radial frozen coordinate [m]
CFD	Computational Fluid Dynamics
D	Jet diameter [m]
H	Jet-solid distance [m]
h	Heat transfer coefficient [$W/(m^2$ K)]
H1	Solid radius [m]
HF	Hydrofluidisation Freezing
HPF	High Pressure-assisted Freezing
IF	Impingement Freezing
L	Domain length [m]
Re	Reynolds number of the jet

1 Introduction

An important part of food industry is represented by freezing of products such as vegetables and meat. Food freezing is a complex problem which needs to take into account several different parameters for a complete description of the process, such as freezing time, food quality, and freezing cost. Among the different freezing techniques available nowadays (for a review of some of these techniques see [1, 2]), historically, commercial freezing of food products was obtained either through cryogenic immersion or mechanical freezing [3, 1]. The two processes are often combined: an initial short immersion step is employed to form a frozen layer that protects the product during transportation and prevents losses in the moisture content during the subsequent slow mechanical freezing [3].

Cryogenic freezing typically requires the use of liquid N_2 or liquid CO_2 [4] and has the highest rate of heat transfer compared to other processes due both to the high temperature gradients between the coolant and the food, and the evaporation of the refrigerant (latent heat of vaporisation). Additionally, the highest rates of heat transfer reached in cryogenic freezing result in the formation (nucleation) of smaller ice crystal inside the solid. This is associated with higher food quality since the ice crystals produced by cryogenic freezing are too small to damage the food structure [5, 6, 7, 8, 9]. However, cryogenic freezing has two main disadvantages: the sudden freezing may induce stresses in the product leading to damage [10], and the volume of cooling liquid required (up to 1 kg of N_2 per 1 kg of processed product [11, 4]) makes this technique expensive.

Mechanical freezing is cheaper than cryogenic freezing, but is less efficient (heat transfer coefficients $h << 50$ W/(m^2 K)). The reduced heat transfer rate leads to the growth of significantly larger ice crystals and thus to a reduced of quality of the final product [11].

As a result, there is a substantial interest for exploring faster and cheaper alternatives for food freezing, which to date resulted in the development of techniques such as Impingement Freezing (IF), High Pressure-assisted Freezing (HPF), and Hydrofluidisation Freezing (HF). Descriptions of these techniques can be found in [1, 7, 6].

Impingement freezing is essentially an improved mechanical freezer [1] in which a cold air jet is perpendicularly directed towards the food, providing a significant increasing of the heat transfer due to the break-up of the fluid boundary layer next to the solid surface [12]. Traditionally, an impingement freezer for food industry would have the following components (Figure 1a) [11]:

- Freezing chamber.
- Grid or conveyor belt on which the produce is placed and transported.
- One or multiple nozzles which supply high speed cooling air. Nozzles can be installed perpendicularly to the belt or at different angles. Additionally, some nozzles can be placed along the conveyor belt to supply air at different temperatures [13, 7].

It is worth noticing that impingement freezing is one of few new techniques which have been fully commercialised [14, 15, 16] due to its cost effectiveness compared to cryogenic freezing and the significantly lower freezing times compared to conventional mechanical freezing. Clearly, air based impingement works best for dense food products with high surface area, since air has low heat capacity compared to other fluids. However, the process is also well suited for rapid surface freezing applications (such as crust freezing) thanks to the enhanced heat transfer and the boundary layer break-up [1]. It was also shown that, for some applications, impingement freezing is able to achieve similar freezing time compared to cryogenic freezing (e.g. for small burgers [17]), without requiring the complex apparatus of the cryogenic process. Furthermore, IF is 62-79% faster and with 36-72% reduced weight loss when compared to conventional freezing, thanks to the higher heat transfer coefficient achievable [11]. Experiments showed that the heat transfer coefficient ranges between $70 - 250$ W/(m^{2}K), depending on the regime of the cooling air [4], which is higher than most of the other forced convection freezing methods [18]. However, it should also be noted that, whilst increasing jet velocity reduces the freezing time, it could also have damaging effects on the mechanical structure of the food [4]. Additional drawbacks of the IF with respect to standard freezing equipment are the higher installation costs and power consumption. However, these are offset by much faster product processing capabilities [16]. IF is also more complex than conventional mechanical freezing and finding the optimal operation parameters for a specific product is often challenging and requires at least a detailed study of conjugate heat transfer and fluid mechanics. Optimisation of this process can only be studied combining experiments and numerical modelling, since analytical relations can only be found for excessively simplified cases.

Generally, in experimental studies, the heat transfer coefficient is measured for both control samples [19] or real food [4] products under impingement conditions. An interesting scenario was considered by [14], who investigated the optimum jet placement. They found that the best freezing conditions can be obtained by placing the jets at approximately 6-8 jet diameters away from the freezing surface. However, extracting accurate measurements and isolating only the phenomena that are most relevant to the process is very difficult under laboratory conditions. Therefore, numerical simulations are a necessary tool for optimisation since, unlike experiments, they allow to study the problem in details and to extract all the available information under controlled conditions, attracting the interest of the food community [20].

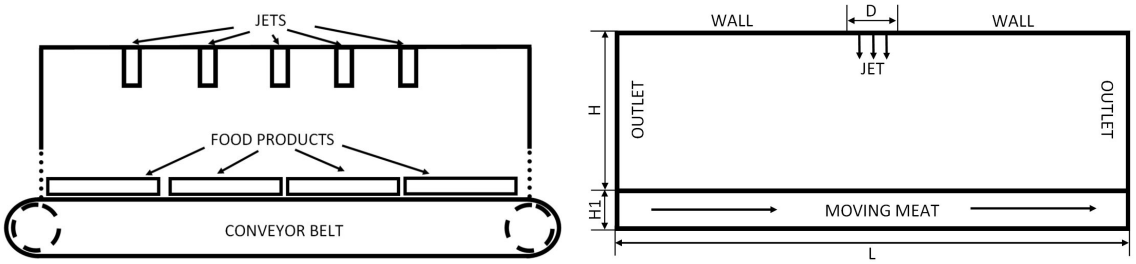

(a) (b)

Figure 1: a) Typical impingement freezing setup. b) Simplified axisymmetric setup for continuous impingement freezing with indicated the relevant dimensions.

In currently available literature, most numerical studies focus their attention exclusively on the food product domain, i.e., heat transfer inside the product for a given heat transfer coefficient [11, 3, 21, 22, 23]. The main objective of these studies was to provide a description of the freezing process in the solid domain, its various associated parameters such as mass diffusion, an essential parameter for porous products (e.g. bread), and its related processes such as recrystallisation [21]. Such single-solid domain modelling approaches require special boundary conditions, information regarding coolant temperature and heat transfer coefficient corresponding to a certain freezing process. Such approaches are clearly unable to model the cooling process of an impinging jet in a satisfactory manner, since they completely disregard the fluid dynamics of the process, which is at the core of IF.

Simultaneous numerical modelling of both the fluid and solid domains has been performed only under certain limiting hypothesis, due to the high requirements in terms of computational resources and software complexity. Olsson et al. [24] and Dirita et al. [25] examined the effect of impinging jet cooling of a cylindrical food product placed on a conveyor belt (Figure 1a) using Computational Fluid Dynamics (CFD). In both cases, the turbulent air flow was described using the k-ω SST model, which is effective in capturing the near-wall fluid dynamics critical for IF [26]. Regarding the interface with the food product, in the case of [24] it was modelled as an isotherm boundary, while [25] used a Conjugate Heat Transfer (CHT) formulation with no phase change. The phase change was omitted purely based on arguments of numerical stability, since the resulting sudden change in thermophysical properties can lead to difficult convergence [21]. This, combined with the non-linear nature of fluid dynamics makes the numerical problem very stiff. Jafari et al. [27] modelled the impinging jet and the solid cooling in axisymmetric coordinates using the CFD commercial software ANSYS FLUENT®, but without phase change and motion of the solid. Therefore, their study results rather limited. Other works considered only a single ideal sample of solid (e.g. a single cylinder) [28].

The goal of this work is to develop a continuous axisymmetric impingement freezing model for food products. Unlike existing similar studies (for example [27]), full phase change in the solid is considered, where the change in the thermal and physical properties with the temperature is prescribed as in [3]. The model we present here provides a good computational compromise between complexity of fluid dynamics calculations and the phase changing of the solid, and is able to predict freezing of continuous dense foods such as sausages, cooked ham, mince. Additionally, the model allows the tuning of multiple parameters such as jet diameter, jet distance from food, food velocity, whilst taking into account freezing and impinging jet processes.

ρ_f	1.569	kg/m^3
C_p	1002.7	J/(kg K)
μ	1.467×10^{-5}	Pa s
Pr	0.728	-

Table 1: Constant properties of air at $T = 225$ K. Here C_p is the heat capacity, μ is the molecular viscosity, ρ_f is the fluid density and Pr is the (non turbulent) Prandtl number. Notice that the heat conductivity κ is calculated employing the definition $Pr = \mu C_p/\kappa$.

2 Numerical model

2.1 Governing equations for the fluid flow

The proposed numerical model is implemented in the opensource C++ library OpenFOAM®, using `chtMultiregionFoam` - a solver for conjugate heat transfer as a basis. The phase change and the thermal and physical properties of the food product (which are not available in the standard OpenFOAM® package) are implemented as a custom library. The turbulent fluid flow is modelled using the RANS (Reynolds Averaged Navier Stokes) equations closed with a k-ω SST turbulence model [29] which was shown to give better predictions compared with other closure models for this kind of problems [30, 31]. The equations solved in the fluid domain are:

Conservation of mass

$$\nabla \cdot (\rho_f \mathbf{u}) = 0 \tag{1}$$

Conservation of momentum

$$\nabla \cdot (\rho_f \mathbf{u}\mathbf{u}) = -\boldsymbol{\nabla} p_{rgh} + \boldsymbol{\nabla} \cdot \boldsymbol{\tau}_{\text{eff}} - (\mathbf{g} \cdot \mathbf{x}) \boldsymbol{\nabla} \rho_f \tag{2}$$

Conservation of energy

$$\nabla \cdot (\rho_f \mathbf{u} h_f) = \boldsymbol{\nabla} \cdot \left(\alpha_{\text{eff}} \boldsymbol{\nabla} h_f\right) - \rho_f \mathbf{u} \cdot \mathbf{g} + \boldsymbol{\nabla} \cdot \left(\boldsymbol{\tau}_{\text{eff}} \cdot \mathbf{u}\right) \tag{3}$$

where $\mathbf{u}$ is the fluid velocity field, p_{rgh} is the pressure without the hydrostatic contribution, ρ_{f} is the fluid density, h_{f} is the fluid enthalpy, $\mathbf{g}$ is the gravitational acceleration, and $\mathbf{x}$ is the spatial coordinate. Furthermore, $\alpha_{\text{eff}} = \alpha_{\text{f}} + \mu_t/(\rho_{\text{f}} \text{Pr}_t)$, where α_{f} is the effective heat diffusivity of the fluid and Pr_t is the turbulent Prandtl number taken to be 0.85 in RANS simulations. The effective deviatoric stress tensor is given by:

$$\boldsymbol{\tau}_{\text{eff}} = \mu_{\text{eff}} \left(\boldsymbol{\nabla}\mathbf{u} + \boldsymbol{\nabla}^T \mathbf{u}\right) \tag{4}$$

with $\mu_{\text{eff}} = \mu + \mu_t$, where μ is the molecular viscosity and μ_t is the dynamic turbulent viscosity and calculated based on the turbulence model [26]. Wall treatment uses a switchable low and high Reynolds approach based on the frictional wall distance:

$$y^+ = y \frac{\sqrt{\tau_w \rho_{\text{f}}}}{\mu_{\text{eff}}} \tag{5}$$

where τ_w is the wall shear stress and y is the distance between the first cell and the wall. The model switches from laminar to turbulent at $y^+ = 11$ [32].

In terms of the fluid properties, incompressible air was used with constant properties at $T = 225$ K which are summarised in table 1. In the study, Reynolds number of the jet is defined as:

$$\mathrm{Re} = \frac{\rho_\mathrm{f} U_{in} \mathrm{D}}{\mu} \tag{6}$$

where U_{in} is the jet inlet velocity and D is the jet diameter (see fig. 1b). This dimensionless number is employed to represent different working conditions of the impingement device.

2.2 Governing equations for the solid

One key idea of this model is represented by the fact that the conveyor speed in the energy equation for the solid is implemented as a convection term. This approach allows to represent moving solid domains without actually moving the mesh, with significant savings in terms of accuracy and stability.

The solid phase is modelled using an enthalpy based energy conservation equation for moving materials [33]:

$$\mathbf{v} \cdot \boldsymbol{\nabla} h_\mathrm{s} = \boldsymbol{\nabla} \cdot (\alpha_\mathrm{s} \boldsymbol{\nabla} h_\mathrm{s}) \tag{7}$$

Here h_s is the solid enthalpy, α_s is the solid heat diffusivity and $\mathbf{v}$ is the conveyor speed in [m/s]. In the rest of the paper we will indicate the conveyor speed in mm/s to simplify the notation of this parameter. The idea is to have a motionless solid phase which avoids the necessity of a moving mesh method. What is moving is the heat within the solid, which is modelled as a flow governed by eq. (7). In particular, the advection of the heat within the solid is identified with the movement of the food on the conveyor belt.

This additional term is implemented as a programmable source into OpenFOAM® and it is discretised implicitly. The formulation presented here allows to obtain a steady-state solution, which significantly reduces the computational time compared to moving mesh methods.

The thermophysical model describing the variation of the material properties with temperature is based on data for burgers reported in [3], assuming 70% water content throughout the study, which gives a freezing temperature of $T_{fz} = 271.7$ K. This thermophysical model, in addition to continuous freezing which is allowed by the temperature advection term, enables the modelling of phase change and the associated heat of fusion effects to the freezing front and heat transfer coefficient. Finally, a working parameter for the conveyor is defined: the solid Péclet number:

$$\mathrm{Pe_s} = \frac{\mathrm{H}_s |\mathbf{v}|}{\alpha_\mathrm{s}^f} \tag{8}$$

Where H_s is the radial length of the solid (see fig. 1b) and $|\cdot|$ indicates the module operator. α_s^f is the thermal diffusivity of the solid at the freezing temperature which, with the thermophysical parameter for the solid we are assuming here, is equal to 0.12 mm^2/s (see table S.1 of the SM). Using a dimensionless number such as $\mathrm{Pe_s}$ allows us to parametrise the working conditions of the conveyor.

2.3 Computational Domain and Grid Independence

The computational domain is a simplification of the real process shown in fig. 1a and is illustrated in fig. 1b. It is aimed at studying the non-linear freezing behaviour caused by a jet-solid interaction. The differential operators in the governing equations (see eqs. (1) to (3) and (7)) were discretised employing finite volume formulation and the interpolation schemes shown in Table 2. Throughout

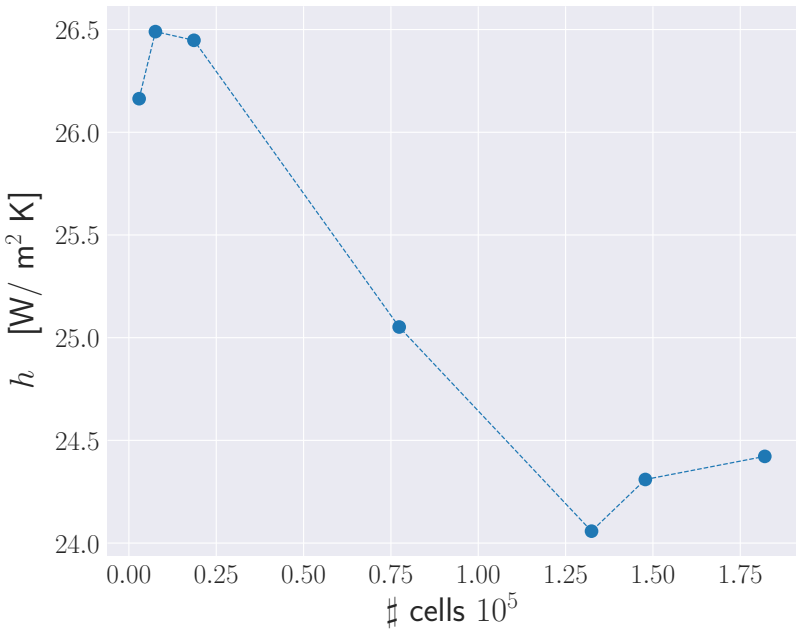

Figure 2: Average Heat transfer coefficient h at the fluid-solid boundary versus number of cells in different meshes.

the study, both jet and solid inlet temperatures were kept constant and equal to $T_{in,\mathrm{f}} = 225$ K and $T_{in,\mathrm{s}} = 274$ K respectively. The computational domain is defined by several geometrical parameters based on the jet diameter D with dimensions respectively equal to: H_s=0.2D, H = 1.8D, L = 7D. Numerical grids were built in OpenFOAM® using the *blockmesh* utility, which allows the generation of orthogonal hexahedral meshes. In the following, we will analyse the freezing process for a variety of scenarios representing different geometrical parameters of the computationl domain.

2.3.1 Grid Independence

Sensitivity of the solutions with respect to the mesh resolution was investigated using the meshes reported in table 3, with operating conditions defined by: $U_{in} = 5$ m/s and $|\mathbf{v}| = 1$ mm/s. These

gradient (∇)	Gauss linear
laplacian (∇^2)	Gauss linear corrected
div(phi,U)	Gauss linearUpwindV grad(U)
div(phi,h) (solid)	Gauss linearUpwind grad(h)
div(phi,h) (fluid)	bounded Gauss upwind
div(phi,k)	Gauss upwind
div(phi,omega)	Gauss upwind

Table 2: Discretisation schemes as from the *fvSchemes* OpenFOAM® dictionary used for simulations.

	Number of cells			
Mesh	Total	Solid	Fluid	$y+_{mean}$
Ex-coarse	4233	663	3570	21.78
Coarse	9000	1500	7500	15.61
Medium	19950	3990	15960	13.38
Medium2	78400	28000	50400	0.72
Fine	133000	49400	83600	0.08
Fine2	148200	49400	98800	0.03
Fine3	182400	49400	133000	0.03

Table 3: Meshes used for the grid independence study.

particular operating conditions result in a large amount of solid material becoming frozen, and therefore, they are a good indicator of the robustness of the algorithm. We define the average heat transfer coefficient, h, as [34]:

$$h = \frac{\dot{q}_{fs}}{T_{in,\mathrm{f}} - T_{fs}} \tag{9}$$

where $\dot{q}_f s$ and T_{fs} represents the total heat exchanged and the average temperature at the interface between fluid and solid respectively, and analyse this parameter as a function of the grid size. We decided to consider h for this analysis as it also represents the quantity which measure the performance of the apparatus. The results reported in fig. 2 show grid convergence in the values of h for grids finer than the one indicated as *Fine* in table 3.

Temperature profile along the fluid-solid interface, reported in figure S.1 of the SM, also shows convergence for the finer grids. It can also be inferred from fig. 2, that the three finer grids predict a very similar heat transfer coefficient whilst lower resolution grids tend to overestimate the performance of the heat transfer in the model. This last observation is also clearly represented in the temperature profile along the fluid-solid interface (see figure S.1 of the SM), where it is shown that the coarser meshes lead to a rather significant overcooling. Thus, it was found that the mesh resolution indicated as *Fine2* (see table 3) is appropriate to conduct the present study. The temperature and velocity fields obtained employing such grid are shown in Figure S.2 of the SM.

3 Results

A parametric study was performed by sampling at eight values of Re in the range $1.604 \times 10^5 \leq \mathrm{Re} \leq 1.604 \times 10^6$ ($3 \leq U_{in} \leq 30$ m/ s) and at seven conveyor speeds in the range $1 \leq |\mathbf{v}| \leq 100$ mm/s. This choice of parameters resulted in a solid Péclet number in the range: $811 \leq \mathrm{Pe_s} \leq 81120$, allowing to consider a variety of scenarios.

We identified two parameters of interest in the description of this process: the dimensionless Freezing Time (dFT), t_{fz}, and the dimensionless Frozen Crust (dFC) F_r. They are both calculated considering the iso-surface at $T = 271$ K in the solid domain (≈ 0.5 K below a freezing point of the solid). The dFT represents the first coordinate, x_{fz}, of the iso-surface just defined along the axial direction (x in our configuration):

$$\tau_{fz} = \frac{x_{fz}}{|\mathbf{v}| t_{\mathrm{L}}} = \frac{x_{fz}}{|\mathbf{v}|} \frac{|\mathbf{v}|}{\mathrm{L}} = \frac{x_{fz}}{\mathrm{L}}. \tag{10}$$

Note that, in our definition, the freezing time τ_{fz} is a dimensionless quantity obtained dividing its dimensional value by the time required for the conveyor to perform one passage through the domain

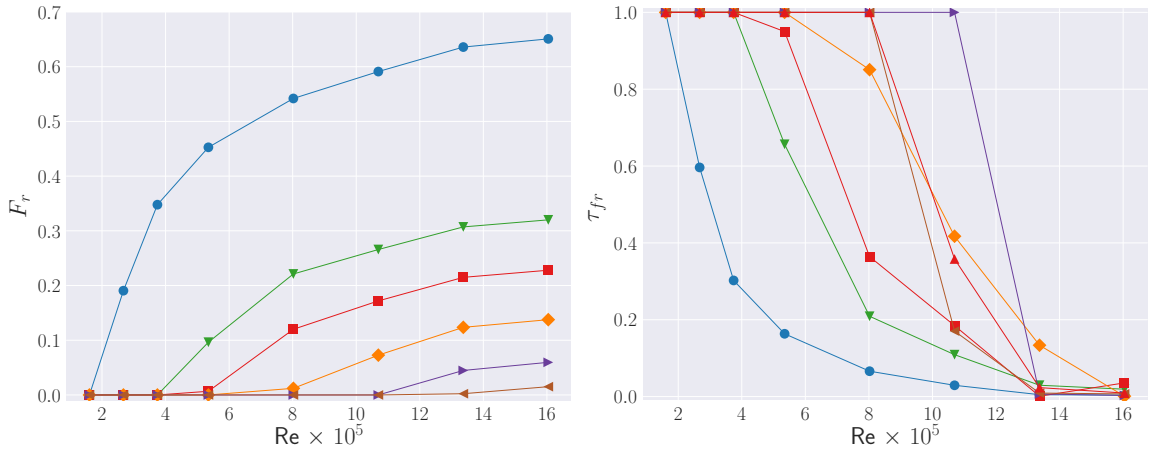

(a) Dimensionless Frozen Crust

(b) Dimensionless Freezing Time

Figure 3: Dimensionless Frozen Crust and Dimensionless Freezing Time associated at various solid Péclet and Reynolds numbers. The different symbols represents: ◯ Pe=811, ▽ Pe=2430, □ Pe=4060, ◊ Pe=8112, ▷ Pe=20280, ◁ Pe=40559, △ Pe=81120. Note that the highest Péclet (Pe=81120) is not shown in plot (a) for clarity, since for this case the value of Fr is zero for each Reynolds considered. The data is for domain H=1.8D. Lines are inserted as a guide for the eye.

$t = \mathrm{L}/|\mathbf{v}|$. τ_{fz} measures the point of the domain (i.e. the position on the conveyor belt) at which the solid starts to freeze (i.e. there is at least a point within the solid domain which overcomes the freezing temperature). A value of $\tau_{fz} = 0$ means that the solid starts to freeze as soon as it enters in the equipment, whereas $\tau_{fz} = 1$ indicates that at the exit of the equipment its outer layer has just reached the freezing temperature. The dimensionless frozen crust (F_r) was calculated using the radial coordinate (the direction y in our configuration), y_{fz}, of the iso-surface at $T = 271$ K in the solid domain at $x = \mathrm{L}$:

$$F_r = \frac{\mathrm{H}_s - y_{fz}}{\mathrm{H}_s} \tag{11}$$

since the zero of our system of coordinates is at the bottom of the frozen domain (i.e. $y = 0$ represents the meat in contact with the belt) y_{fz} is the height of the solid not frozen. A value of $F_r = 0$ indicates that no frozen crust is formed when the meat reaches the outlet of the equipment, whereas $F_r = 1$ means that the solid is completely frozen.

In fig. 3 the results for dFT and dFC are reported. First thing to notice is that the initial stable freezing time reported in fig. 3b shows that for low Reynolds numbers no freezing occurs while the solid is transported through the domain. At $\tau_{fz} = 1$ the process was only able to overcome the latent heat of solidification of the solid, without any appreciably freezing crust formed. We can determine that there is no crust formed by looking at fig. 3a. At the lowest Reynolds number our calculations show a dFC of $F_r = 0$, indicating that the solid did not freeze appreciably, and higher forced convection is required to overcome the latent heat of freezing. On the other hand, the results reported at the highest Reynold number show that the freezing process is almost instantaneous and leads to a significant frozen crust formation in the majority of the situations. Interestingly, it can be observed that no significant frozen crust layer is formed for the highest Péclet number considered $\mathrm{Pe_s} = 81120$, i.e $F_r = 0$ for every Re considered. However, from fig. 3b, we can see for the case

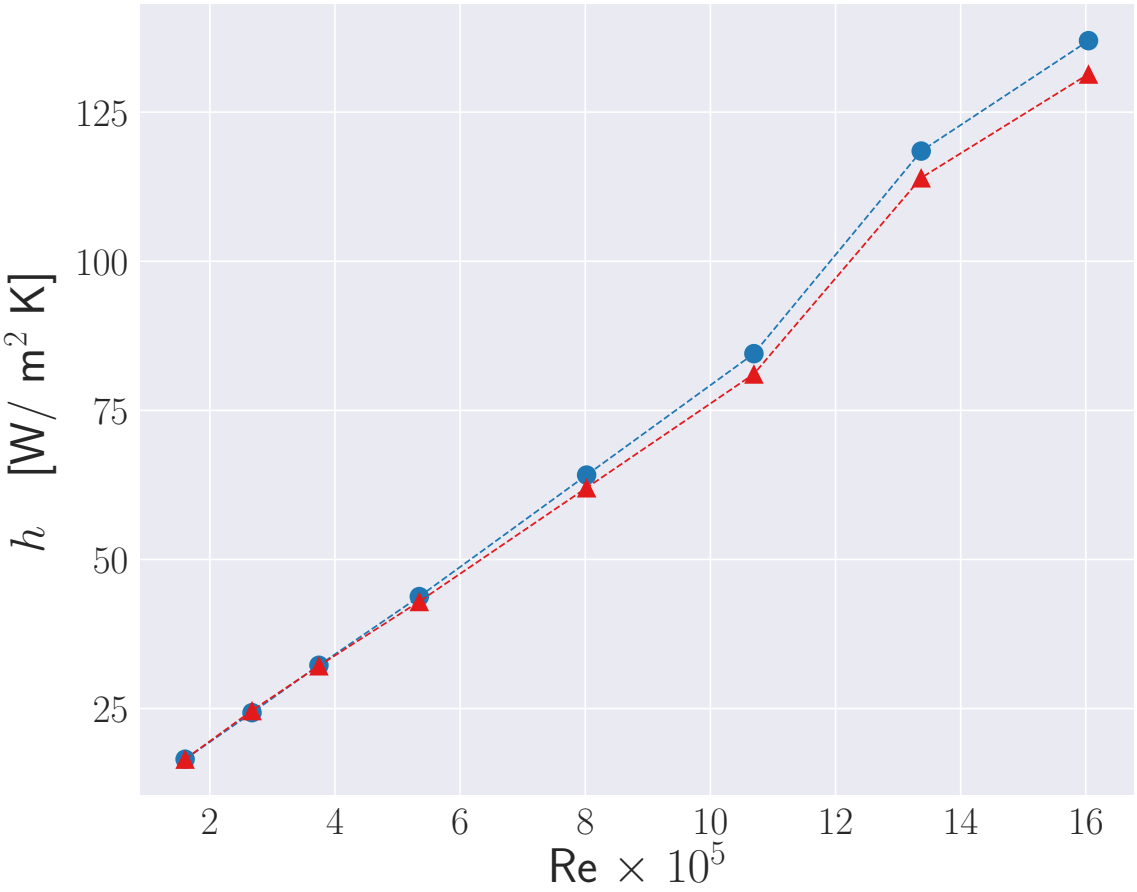

Figure 4: Heat transfer coefficient h as function of Reynolds number for two different values of the Péclet number: ◯ Pe=811, △ Pe=81120. The data refer to the domain of H=1.8D. Lines are inserted as guide for the eye.

$Pe_s = 81120$ that for Re$> 10^6$ the dimensionless freezing time is smaller than one. This last fact can be explained by considering that for higher Reynolds number the latent heat of freezing is overcome and the solid start to freeze (i.e. the freezing temperature is quickly reached), but the velocity of the conveyor belt is so high that the solid does not have time to develop a freezing crust of an appreciable dimension. These kind of conclusions shows the potential of this approach, which is able to guide the exploration of the parameter space in order to optimise this process for every kind of products.

The heat transfer coefficient for the lowest and highest Péclet numbers considered ($Pe_s = 811$ and $Pe_s = 81120$) is shown in fig. 4. Interestingly, the conveyor speed does not seem to have an appreciable effect on the heat transfer. This result seems counter-intuitive, since one would think that the additional shear created at the fluid-solid interface should increase fluid mixing and consequently increase the heat transfer coefficient. However, we have to consider that the meat has a low thermal conductivity which has the effect of keeping the heat transfer coefficient almost

constant across the whole range of operating conditions. For higher values of the Reynolds number a small decrease in h can be observed for the case of $\mathrm{Pe_s} = 81120$ with respect the simulation with $\mathrm{Pe_s} = 811$. This effect is related to the difference in frozen crust temperature between the two operating conditions. The effect of the quick freezing discussed above can also be seen in Figure 4 at the two highest Reynolds numbers, where a change of slope takes place, when the latent heat of fusion at the solid-fluid interface is overcome.

The results just discussed also show that a more detailed analysis is necessary to investigate the two dominant parameters of the impingement freezing domain: the jet distance from the solid (H) and solid material thickness (H_s). We analyse them in next sections for the two limiting values of the Péclet number ($\mathrm{Pe_s} = 811$ and $\mathrm{Pe_s} = 81120$).

3.1 Influence of the jet diameter

Effects of the distance between the jet nozzle and the solid have been considered since [14], that reported an optimum value of H between 6 and 8.

In this subsection, the computational domain is modified by reducing the jet diameter two and four times ($\mathrm{D_1} = 0.5\mathrm{D}$ and $\mathrm{D_2} = 0.25\mathrm{D}$), effectively obtaining the new values of $\mathrm{H} = 3.6\mathrm{D_1}$ and $\mathrm{H} = 7.2\mathrm{D_2}$ for the relation with H. It should be noted, that all the other geometrical parameters were left identical to the original domain. This allows to keep a solution similarity.

Contour plots for the three domains considered are shown in fig. 5. By looking at the amount of frozen solid on the bottom of the contour plots, these results suggest that, for the same value of the Reynolds number, the further away the jet is from the solid domain the quicker is the freezing process. Additionally, the fluid bulk region which develops between the interface and the jet inlet, is larger for larger values of D. This means that for smaller values of D the region near the solid experiences a higher velocity field that results in enhanced fluid mixing and heat transfer, leading to a more efficient freezing. In terms of heat transfer coefficient, this effect is shown in fig. 6. The largest heat transfer coefficient results from moving the jet inlet away from the solid in agreement with results from [14]. In particular, the heat transfer coefficients in the case of $\mathrm{H} = 7.2\mathrm{D}$ is more than doubled than for the $\mathrm{H} = 1.8\mathrm{D}$ domain.

In fig. 7, freezing time and crust thickness for the case $\mathrm{H} = 0.25\mathrm{D}$ are reported (the same results for the intermediate case of $\mathrm{H} = 0.5\mathrm{D}$ are shown in Figure S.4 of the Supplementary Materials (SM)). Comparing the freezing time and crust thickness, it can be noticed that increasing the distance of the jet from the solid results in both faster freezing time and deeper crust formation. For the highest value of the Péclet ($\mathrm{Pe_s} = 81120$) we obtain profiles similar to those in the original domain, and thus in the formation of a very thin frozen crust despite an almost instant freezing time. For both $\mathrm{H} = 3.6\mathrm{D}$ and $\mathrm{H} = 7.2\mathrm{D}$ the crust is still significantly larger with respect to the case with $\mathrm{H} = 1.8\mathrm{D}$ (see fig. 7b and fig. S.4a of the SM). This last fact opens the possibility to optimise the freezing process by just changing the position of the impinging jet. However, an interesting nonlinear behaviour can be seen at $\mathrm{H} = 7.2\mathrm{D}$ and $\mathrm{Pe_s} = 811$ (see Figure 7b) where a stabilisation in dFC is observed at the highest Reynolds numbers. This stabilisation indicates that for a specific solid thickness and conveyor velocity, a critical *Reynolds jet-to-solid* distance can be derived. This parameter can be defined as the distance over which the impingement effect sharpens, resulting in an inefficient cooling.

3.2 Influence of the solid thickness

In this section, we study the influence of different solid thicknesses on the freezing performance. We reduce the solid domain diameter (H_s) by half (we remind here that we are considering an

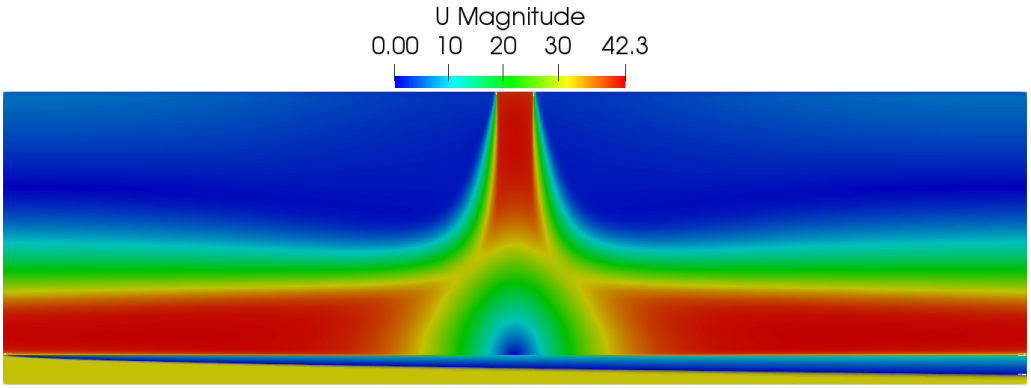

(a) D_1=0.25D

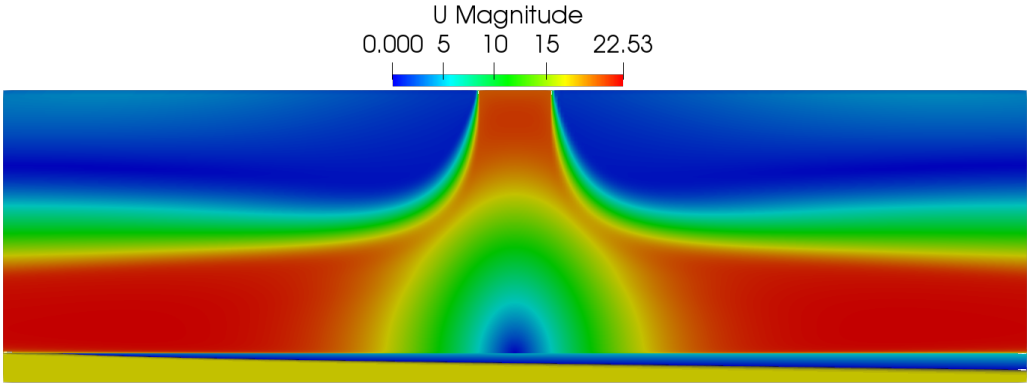

(b) D_2=0.5D

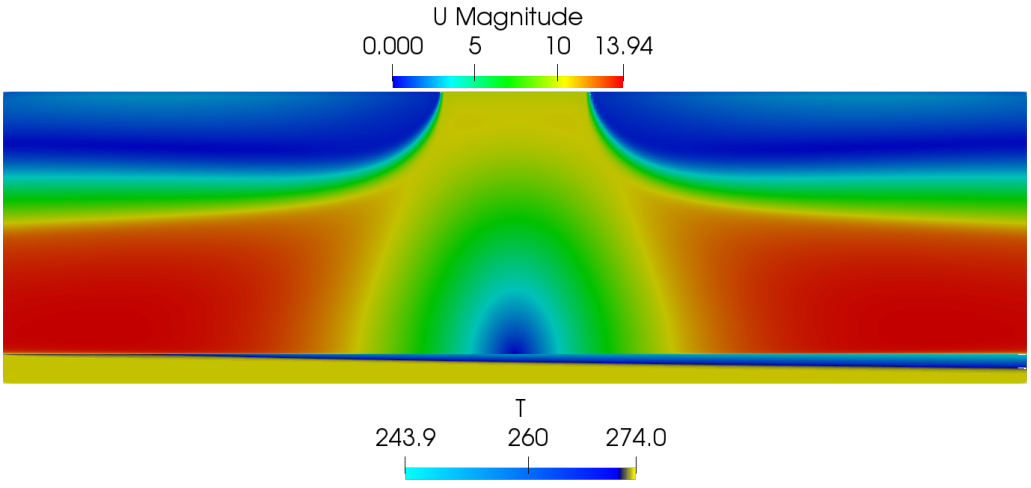

(c) D

Figure 5: Three computational domains at $\mathrm{Re} \underline{\underline{12}} 5.4 \times 10^5$, $\mathrm{Pe_s} = 811$ using the indicated jet-diameter/distance to the solid ratios.

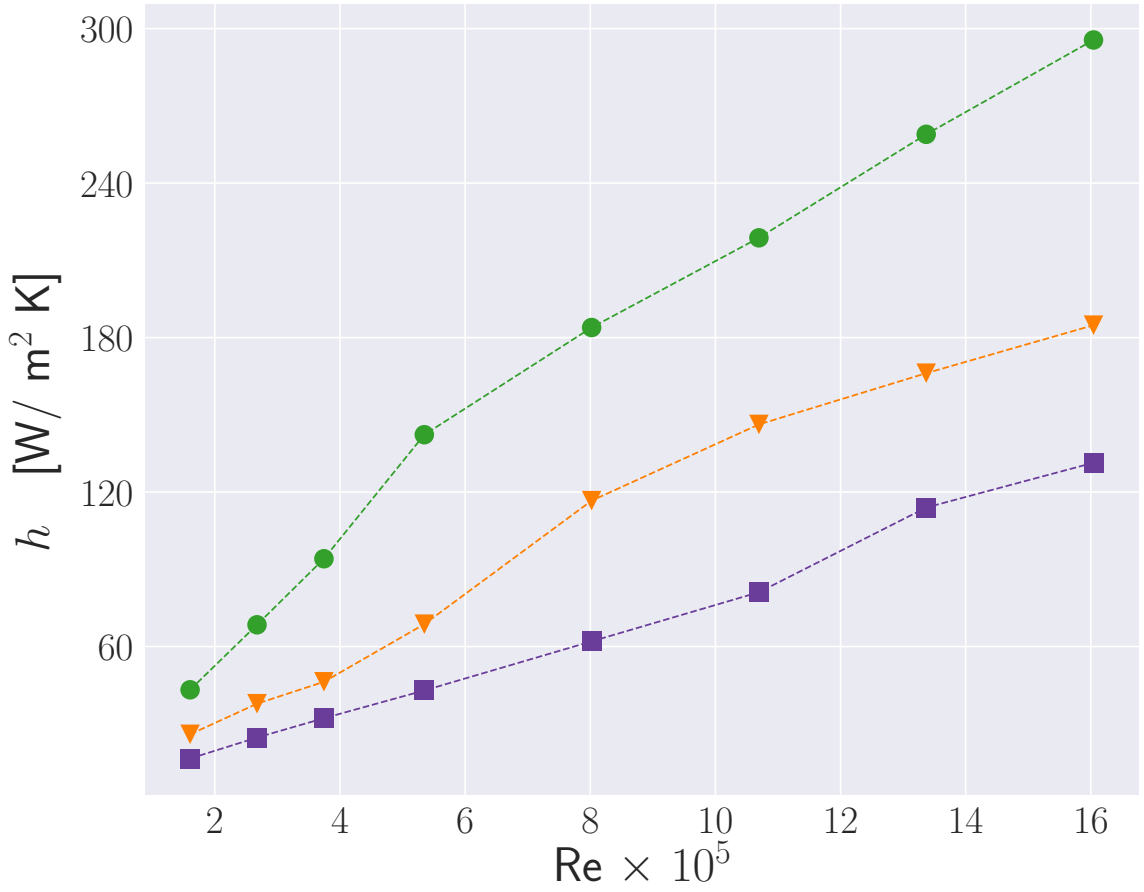

Figure 6: Heat transfer coefficient at $Pe_s = 81120$ using different jet diameter to the distance from the solid: ◯ 0.25D, ▽ 0.5D, □ D. Lines are inserted as guide for the eye.

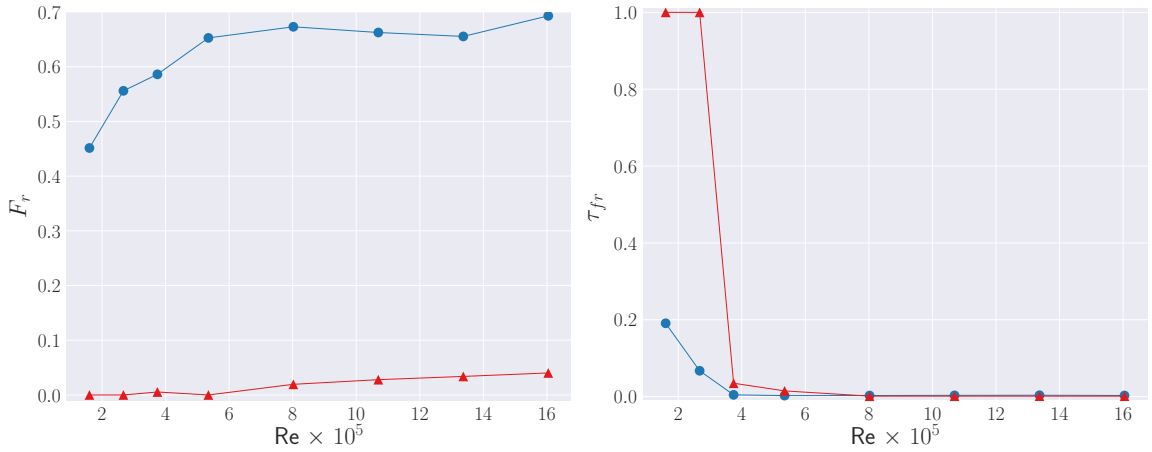

(a) Dimensionless Frozen Crust

(b) Dimensionless Freezing Time

Figure 7: Dimensionless Frozen Crust and Dimensionless Freezing Time associated for the configuration with D_2=0.25D, corresponding to H=7.2D, at different solid Péclet and Reynolds numbers. The different symbols represents: ◯ Pe=811, △ Pe=81120. Lines are inserted as a guide for the eye.

axisymmetric geometry, with the axial dimension being the direction x and the radial dimension the direction y) , compared to the one reported in earlier sections, obtaining a new solid thickness $H'_s = 0.5H_s$. Figure 8 illustrates the results at $Pe_s = 811$.

Comparison with the results in fig. 5c reveals which are the differences between the two domains. In the case of a thinner solid, the process is capable of complete freezing (as shown by the solid at the outlet in fig. 8). This behaviour is clearly represented in fig. 9, where dFC and dFT are reported. We can observe consistent behaviour across a wide range of Reynolds numbers with the complete freezing that starts as soon as Re=10^5. Compared to the results in fig. 3 at $Pe_s = 811$, freezing is observed to take place at lower Reynolds numbers and at shorter axial coordinates. This shows a dependence of the freezing characteristics from the solid diameter and the need to specifically tune the process for different products.

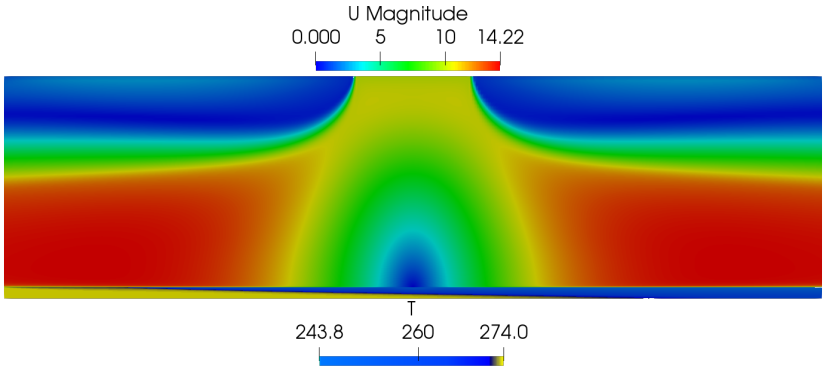

Figure 8: Impingement freezing result at Re = 5.348×10^5, $Pe_s = 811$ using a 50% thinner solid material domain using a jet diameter to solid distance ratio of H=3.6D.

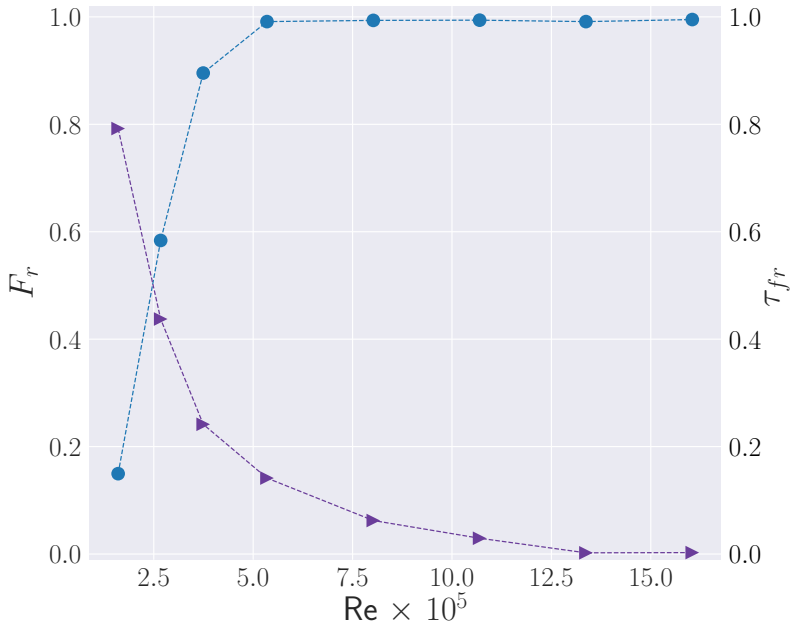

Figure 9: Dimensionless Frozen Crust (◯) and Dimensionless Freezing Time (▷) in the half radius domain (H'_s) as a function of the Reynolds number for $Pe_s = 811$. Lines are inserted as guide for the eye.

4 Conclusions

A numerical model for axial impingement freezing of food products on a moving conveyor is proposed. The model is able to capture phase change, which is critical in the thermophysical description of the freezing process. The model was implemented in the finite volume open-source library OpenFOAM® as a custom solver and its numerical convergence is presented in an industrial application. Key dimensionless parameters were identified to describe the performance of the freezing model. Additionally, a parametric study to investigate the process efficiency under different operating conditions and geometrical configurations of the potential freezing apparatus was considered. The key findings of the study can therefore be summarised by:

- High Reynolds numbers are required to overcome the effects of the latent heat of freezing. The effect becomes more pronounced at high conveyor speeds, in which larger velocities of the solid do not leave sufficient time for the frozen layer to penetrate in depth.
- With our model we re-obtain the expected behaviour of the freezing process. Dimensionless Freezing Time and Crust are dependent on the solid material thickness. By halving the solid domain radius, the complete freezing of the food product was observed as it moves along the domain. Thus, this case requires a significantly lower fluid flow speed and overall heat transfer coefficient.

A necessary future extension of the model presented here requires the use of more refined turbulence models such as the LES [30]. Future studies may also include the investigation of more complicated 3-dimensional geometries as well as the generalisation to heterogeneous and anisotropic food products through the use of improved thermophysical models.

Acknowledgements

The authors would like to thank University of Nottingham Hermes fund for sponsoring the research.

References

[1] C. James, G. Purnell, and S. J. James. A Review of Novel and Innovative Food Freezing Technologies. *Food and Bioprocess Technology*, 8(8):1616–1634, aug 2015.

[2] J. Evans. Emerging refrigeration and freezing technologies for food preservation. In *Innovation and Future Trends in Food Manufacturing and Supply Chain Technologies*, pages 175–201. Elsevier, 2016.

[3] M. E. Agnelli and R. H. Mascheroni. Cryomechanical freezing. A model for the heat transfer process. *Journal of Food Engineering*, 47(4):263–270, 2001.

[4] V. Soto and R. B. Orquez. Impingement jet freezing of biomaterials. Technical report.

[5] W. E. L. Spiess. Impact of freezing rates on product quality of deep-frozen foods. *Food Process Engineering, Applied Science, London*, pages 689–694, 1980.

[6] T. Marazani, D. M. Madyira, and E. T. Akinlabi. Investigation of the Parameters Governing the Performance of Jet Impingement Quick Food Freezing and Cooling Systems - A Review. *Procedia Manufacturing*, 8:754–760, 2017.

[7] L. D. Kaale, T. M. Eikevik, T. Rustad, and K. Kolsaker. Superchilling of food: A review, dec 2011.

[8] K. P. Poulsen. The freezing process under industrial conditions. *Science et Technique du Froid (IIR)*, 1977.

[9] P. Nesvadba. Thermal properties and ice crystal development in frozen foods. *Frozen food science and technology*, page 1, 2008.

[10] G. H. Zhou, X. L. Xu, and Y. Liu. Preservation technologies for fresh meat - A review, sep 2010.

[11] V. O. Salvadori and R. H. Mascheroni. Analysis of impingement freezers performance. *Journal of Food Engineering*, 54(2):133–140, sep 2002.

[12] M. Newman. Cryogenic impingement freezing utilizing atomized liquid nitrogen for the rapid freezing of food products. In *Rapid Cooling of food, Meeting of IIR Commission C*, volume 2, pages 145–151, 2001.

[13] R. C. Lee and M. K. Sahm. Impingement jet freezer and method, April 21 1998. US Patent 5,740,678.

[14] A. Sarkar and R. P. Singh. Modeling flow and heat transfer during freezing of foods in forced airstreams. *Journal of food science*, 69(9):E488–E496, 2004.

[15] A. Sarkar and R. P. Singh. Air impingement technology for food processing: Visualization studies. *LWT - Food Science and Technology*, 37(8):873–879, 2004.

[16] N. Winney. From the field to the supermarket–Post harvest cooling, part 2 of 4. *Cold Chain*, 2012:20–26, 2012.

[17] S. Sundsten, A. Andersson, and E. Tornberg. The effect of the freezing rate on the quality of hamburgers. In *Rapid cooling of food, meeting of IIR Commission C*, volume 2, page 2001, 2001.

[18] P. Dempsey and P. Bansal. The art of air blast freezing: Design and efficiency considerations. *Applied Thermal Engineering*, 41:71–83, 2012.

[19] B. A. Anderson and R P. S. Effective heat transfer coefficient measurement during air impingement thawing using an inverse method. *International Journal of Refrigeration*, 29(2):281–293, 2006.

[20] R. A. Lemus-Mondaca, A. Vega-Gálvez, and N. O. Moraga. Computational simulation and developments applied to food thermal processing. *Food Engineering Reviews*, 3(3-4):121–135, 2011.

[21] Q. T. Pham. Modelling heat and mass transfer in frozen foods: a review, sep 2006.

[22] F. Erdogdu, A. Sarkar, and R. P. Singh. Mathematical modeling of air-impingement cooling of finite slab shaped objects and effect of spatial variation of heat transfer coefficient. *Journal of Food Engineering*, 71(3):287–294, 2005.

[23] Q. T. Pham. Freezing time formulas for foods with low moisture content, low freezing point and for cryogenic freezing. *Journal of Food Engineering*, 127:85–92, 2014.

[24] E. E. M. Olsson, L. M. Ahrne, and A. C. Trägårdh. Heat transfer from a slot air jet impinging on a circular cylinder. *Journal of Food Engineering*, 63(4):393–401, 2004.

[25] C. Dirita, M. V. De Bonis, and G. Ruocco. Analysis of food cooling by jet impingement, including inherent conduction. *Journal of Food Engineering*, 81(1):12–20, jul 2007.

[26] F. R. Menter, M. Kuntz, and R. Langtry. Ten years of industrial experience with the SST turbulence model. *Turbulence, heat and mass transfer*, 4(1):625–632, 2003.

[27] M. Jafari and P. Alavi. Analysis of food freezing by slot jet impingement. *Journal of Applied Sciences*, 8(7):1188–1196, 2008.

[28] E. E. M. Olsson, H. Janestad, L. M. Ahrné, A. C. Trägårdh, and R. P. Singh. Determination of local heat-transfer coefficients around a circular cylinder under an impinging air jet. *International Journal of Food Properties*, 11(3):600–612, 2008.

[29] S. Chandrasekhar. *Hydrodynamic and hydromagnetic stability*. Courier Corporation, 2013.

[30] A. Dewan, R. Dutta, and B. Srinivasan. Recent trends in computation of turbulent jet impingement heat transfer. *Heat Transfer Engineering*, 33(4-5):447–460, 2012.

[31] N. Zuckerman and N. Lior. Jet impingement heat transfer: physics, correlations, and numerical modeling. *Advances in heat transfer*, 39:565–631, 2006.

[32] F. M. White. *Fluid Mechanics*. Mcgraw-Hill, 2011.

[33] Joel H Ferziger, Milovan Perić, and Robert L Street. *Computational methods for fluid dynamics*, volume 3. Springer, 2002.

[34] D. Góral and F. Kluza. Heat transfer coefficient in impingement fluidization freezing of vegetables and its prediction. *International Journal of Refrigeration*, 35(4):871–879, 2012.